Life consumption of a MMC-STATCOM Supporting Wind Power Plants: Impact of the Modulation Strategies

A. F. Cupertino, J. V. M. Farias, H. A. Pereira and R.O.Sousa

Published in:

Microelectronics Reliability

DOI (*link to publication from Publisher*):

10.1016%2Fj.microrel.2018.06.111

Publication year:

2018

Document Version:

Accepted author manuscript, peer reviewed version

Citation for published version:

A. F. Cupertino,J.V.M.Farias, H. A. Pereira and R.O.Sousa"Life consumption of a MMC-STATCOM Supporting Wind Power Plants: Impact of the Modulation Strategies,"Microelectronics Reliability, vol88-90,pp.1063-1070, September 2018.
doi: 10.1016%2Fj.microrel.2018.06.111

Life consumption of a MMC-STATCOM Supporting Wind Power Plants: Impact of the Modulation Strategies

R. O. de Sousa[a], J. V. M. Farias[b], A. F. Cupertino[c,d], H. A. Pereira[b]

[a]*Graduate program in Electrical Engineering, Federal Center for Technological Education of Minas Gerais,Belo Horizonte, Brazil*
[b]*Department of Electrical Engineering, Federal University de Viçosa, Viçosa, MG, Brazil*
[c]*Graduate program in Electrical Engineering, Federal University of Minas Gerais, Belo Horizonte, MG, Brazil*
[d]*Department of Materials Engineering, Federal Center for Technological Education of Minas Gerais,Belo Horizonte, Brazil*

Abstract

The increasing penetration of Wind Power Plants (WPPs) has several impacts on the power system operation, such as voltage instability. Under such conditions, the literature suggests the use of static synchronous compensators (STATCOMs). Additionally, the Modular Multilevel Converter (MMC) is featured as a very suitable topology for STATCOM application. Therefore, this paper contributes to the knowledge in the field by analyzing the effect of the modulation strategies in losses and lifetime of a 17 MVA MMC-STATCOM. These analyses use two well-know modulation strategies: Phase-Shifted Pulse-Width Modulation (PS-PWM) and Nearest-Level Control (NLC). The results indicate that both strategies have similar conduction losses, although PS-PWM has almost twice more switching losses. As a result, the PS-PWM has annual energy consumption 31.4% higher than NLC. Regarding the lifetime evaluation, the results show superior performance for the NLC, for cell-level and system-level, with lifetime 25.6 and 10.6 times longer than PS-PWM, respectively.

1. Introduction

The increasing penetration of wind power and growing size of Wind Power Plants (WPPs) have a significant impact on the power system operation and pose technical challenges to the improvement of voltage stability. In fact, large WPPs are mainly located in areas far from load centers, which results in low short-circuit ratio (SCR) at the point of common coupling (PCC) [1]. Under such conditions, the technical literature suggests the use of the Static Synchronous Compensators (STATCOM) [2, 3]. The STATCOM device is connected in parallel with the electric grid, as illustrated in Fig. 1, and can provide/absorb reactive power, thus controlling the bus voltage level and improving reliability, stability and power quality in medium and high voltage distribution networks [4].

Moreover, the modular multilevel converter (MMC) is considered as the next generation converter for medium and high voltage grid STATCOM applications [5, 6]. The MMC combines excellent harmonic performance and low switching frequency. Additionally, the MMC structure is modular and fault-tolerant, resulting in high reliability and design flexibility [5, 7].

An important issue related to MMC is the employed modulation strategy [8]. In this context, different strategies have been proposed in the literature, resulting in different switching patterns and power losses [6]. For instance, references [9, 10, 11] present comparisons among modulation strategies in terms of power losses, thermal stress, output current THD and number of switching events. Nevertheless, a comparison of the modulation strategies regarding the converter life consumption was not previously reported.

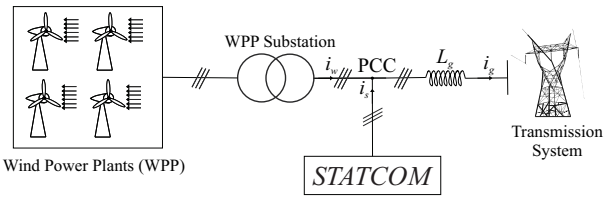

Figure 1: Schematic system diagram.

In this context, this paper contributes to the knowledge in the field by comparing two very popular modulation strategies employed in MMC: Phase-Shifted Pulse-Width Modulation (PS-PWM) and Nearest-Level Control (NLC) [8]. These strategies are compared in terms of power loses and life consumption of the power

semiconductors. The analysis is based on mission profile of reactive power measured in South-eastern Brazil. Component-level and system-level reliability are evaluated through Monte Carlo simulations.

This paper is outlined as follows. Section 2 presents the MMC topology and modulation strategies studied. Section 3 describes the lifetime evaluation method. Section 4 presents the case study and the parameters of the simulated model as well the obtained results. Finally, the conclusions of this work are stated in Section 5.

2. Topology and Modulation Strategies

The STATCOM topology analyzed in this work is the Double-Star Chopper Cell MMC (DSCC-MMC), presented in Fig. 2. In this topology, there are N cells per arm and each cell contains four semiconductor devices (S_1, S_2, D_1 and D_2) and a capacitance C. In general, there is a switch S_T in parallel with the cell bypassing it in case of failures. The arm inductance is represented by L_{arm} and the grid inductance, by L_g. Moreover, i_u and i_l are the upper and lower arm currents, respectively. The grid voltage and current are represented by v_g and i_g, respectively.

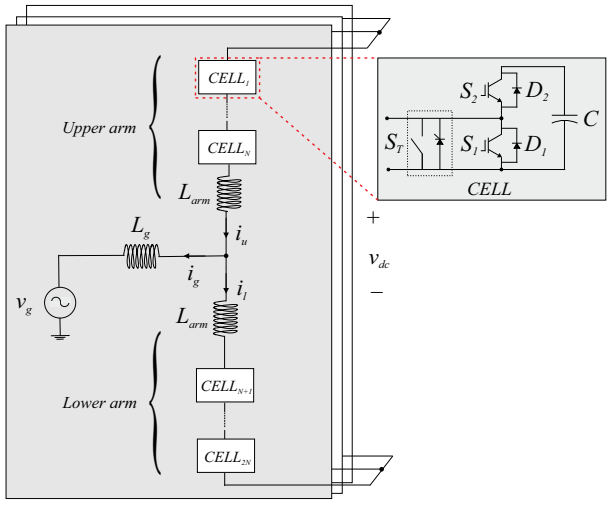

Figure 2: Schematic of the DSCC-MMC STATCOM.

Regarding the control strategy, this work uses the same approach of [12], which employs the following controls: output current control, circulating current control and individual balancing control. The output current and circulating current control are related with the MMC topology and do not depend on the modulation strategy. On the other hand, each modulation strategy employs different individual balancing control structures [8].

Regarding the modulation strategies, two different approaches are compared: PS-PWM and NLC. PS-PWM is a technique in which the cells are controlled independently. The voltage reference waveform is produced for each cell by the control actions of the output current control, circulating current control and individual balancing control, which are added and normalized. As illustrated in Fig. 3, each cell voltage reference is compared with a carrier triangular which generates the switching pattern for the corresponding cell [6]. The N arm carriers are equally phase shifted inside half period. Additionally, a phase displacement between upper and lower arms is inserted in order to obtain the $2N+1$ level modulation [13].

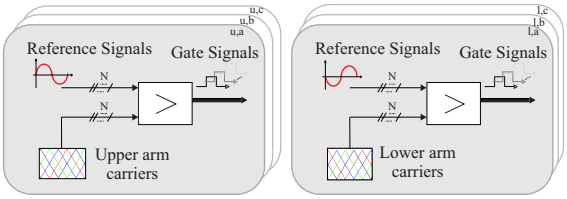

Figure 3: Schematic of PS-PWM strategy.

The main goal of the NLC, as shown in Fig. 4, is to sample, with the nearest available level, the reference signal. Besides, this reference is normalized and multiplied by N before sampling. The nearest available level can be formulated mathematically by applying the $round(x)$ function. Furthermore, the NLC requires a sorting algorithm to ensure cell-energy balancing. In this work, the cell tolerance band (CTB) algorithm is employed [8, 14].

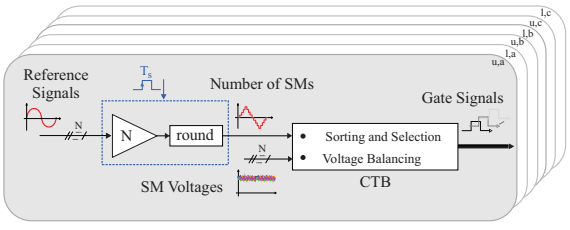

Figure 4: Schematic of NLC strategy.

Furthermore, the switching frequency should be minimized, in order to minimize the switching losses. In this context, the literature recommends for the PS-PWM the switching frequency of 3.5 times the line frequency [12, 15]. However, even with this frequency, the PS-PWM has unnecessary cell transitions [16]. For this

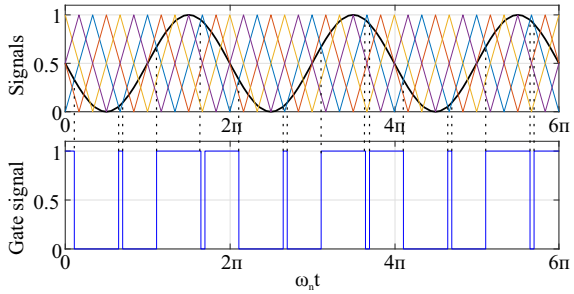

Figure 5: Operation of PS-PWM.

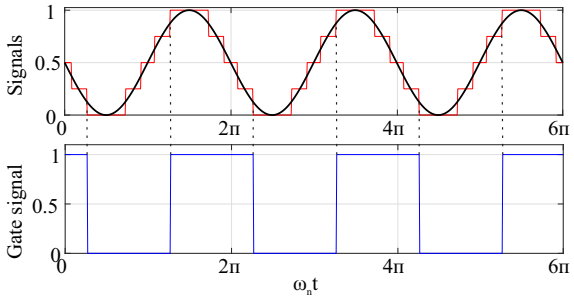

Figure 6: Operation of NLC.

reason, the NLC [17] emerged as an alternative, since it works at lower frequencies, compared to PS-PWM. Indeed, the NLC can results in a steady-state switching frequency as low as line frequency [8].

As an example, Fig. 5 and Fig. 6 illustrate the modulation process for PS-PWM and NLC, respectively, considering an unlimited capacitance and 4 cells per arm. As observed in Fig. 5, for the PS-PWM, the switching is carried out every time the carrier signal is lower than the reference, independently of the need. On the other hand, Fig 6 shows that the switching frequency is the same as, the reference signal. Although this example is for an unlimited capacitance, according to the literature, the NLC operates with lower switching frequency than PS-PWM. Therefore, the NLC tends to have lower switching losses and less stresses on the power devices during the MMC operation.

3. Lifetime Evaluation Procedure

The lifetime evaluation flowchart is shown in Fig. 7. The lifetime evaluation procedure is focused on the semiconductor devices. The complete analysis including capacitors, printed circuit boards and other components is out the scope of this work.

Measurements of reactive power (Q) and ambient temperature (T_a) mission profiles are employed. The losses in the semiconductor devices are obtained from look-up tables based on the data provided in datasheets. This work employs the hybrid thermal model proposed by [18, 19] in order to estimate the junction (T_j) and case temperature (T_c) of each power device. In addition, it is considered one heatsink for each cell.

Afterwards, it is necessary to employ a cycle counting algorithm, in order to convert the temperature profiles in regular series with constant average value ($T_{[j,c]m}$), peak ($\Delta T_{j,c}$) and heating time (t_{on}). This task is performed by a rainflow algorithm [20, 21].

The power device lifetime is usually expressed in terms of Life Consumption (LC), which indicates how much life of the device has been consumed or damaged. The LC is obtained by using the Miner's rule [20], as follows:

$$LC = \sum_i \frac{n_i}{N_{f,i}}, \tag{1}$$

where n_i is the number of cycles obtained from rainflow algorithm and N_f is the number of cycles to failure obtained for each stress condition. In this work, N_f is evaluated through the lookup tables provided by ABB for Hi-Park power modules [22]. This model analyzes N_f in all critical joints of the modules using 10% failure rate approach (B_{10} lifetime). In addition, LC is computed separately for bond wire, base plate solder and chip solder and for each diode and IGBT [23, 24].

Furthermore, in the previous evaluation, a fixed value of time to failure under a certain operating condition is obtained considering an ideal case in which all power devices fail at the same time. However, in fact, the parameters could have variations due to the manufacturing process and the variation in the stresses [21]. Therefore, [25] uses a Monte Carlo analysis, with the goal of computing damage probability distribution.

The Monte Carlo analysis application first requires transforming the dynamic values, $T_{[j,c]m}$, $\Delta T_{j,c}$ and t_{on}, into equivalent static values, $T'_{[j,c]m}$, $\Delta T'_{j,c}$ and t'_{on}, since dynamic parameters cannot easily be modeled with a distribution function. Moreover, the static values should result in the same lifetime when used to the lifetime evaluation process [21].

With the equivalent static values modeled by a normal distribution, parameter variations are introduced into the lifetime model (see Fig. 7). In addition, Monte Carlo analysis with population of 50.000 samples is simulated with the lifetime model. Then, the lifetime yield for each sample is obtained and fitted with the Weibull probability distribution $f(x)$ [21]. In this context, $f(x)$ can be expressed by a probability density function (PDF).

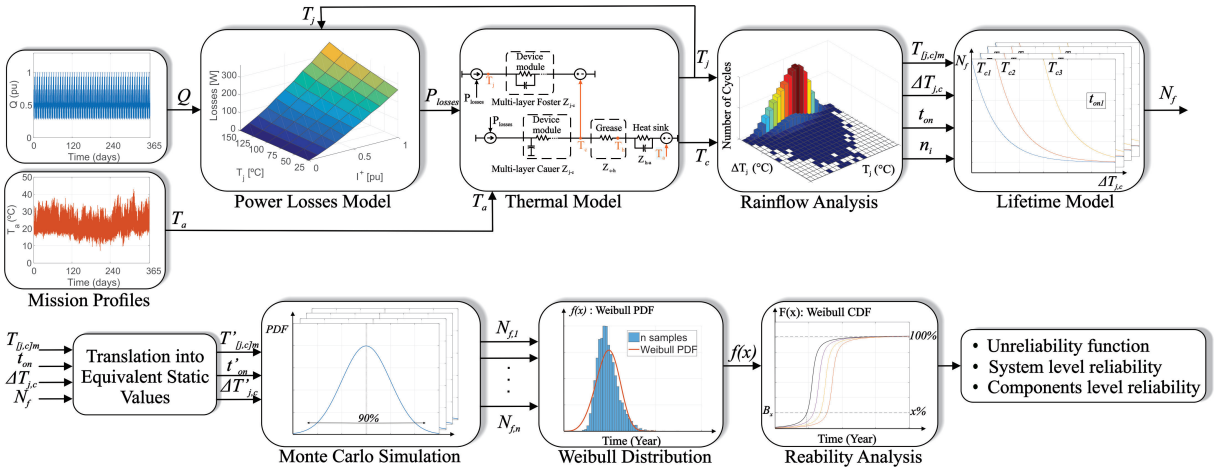

Figure 7: Lifetime evaluation flowchart.

The reliability of the power device can be evaluated by considering the cumulative density function (CDF) of the Weibull distribution which is the integral of PDF ($F(x)$), where x is the operation time. The CDF is also called unreliability function and represents the proportion of population failure as a function of time. Thus, from $F(x)$, the power device lifetime can be predicted [21].

Finally, in order to obtain a system-level reliability assessment based on the component-level, first, it is calculated the unreliability function for each MMC cell, as follows:

$$F_{cell}(x) = 1 - \prod_{i=1}^{4} (1 - F_{D,i}(x)) \tag{2}$$

where $F_{D,i}(x)$ is unreliability function of each device in the cell (S_1, S_2, D_1 or D_2). From Eq. (2), the system-level (MMC) can be calculated as:

$$F_{MMC}(x) = 1 - \prod_{n=1}^{6N} (1 - F_{cell,n}(x)) \tag{3}$$

4. Effect of modulation on lifetime

In the case study, it is considered a 17 MVA STATCOM with 17 cells per arm, cell capacitance 5 mF, arm inductance 4.5 mH, connected to a 60 Hz network with line voltage of 13.8 kV at the point of common coupling (PCC). It is also used an ABB IGBT part number 5SND 0500N330300 of 3.3kV-500A. In order to validate the proposed design methodology and estimate the lifetimes, a simulation model was implemented using the PLECS and MATLAB software systems.

Fig. 8(a) shows the conduction and switching losses for different operation conditions. These losses were estimated considering 40 °C as ambient temperature and $0.075K/W$ as heatsink resistance. As observed in Fig. 8(a), the conduction losses are almost the same for both strategies. However, the PS-PWM presents switching losses 1.95 times higher than NLC. This fact is justified by the effective switching frequency, illustrated in Fig. 8(b) for the same operation conditions. Indeed, the switching frequency is lower for NLC for all operation conditions presented.

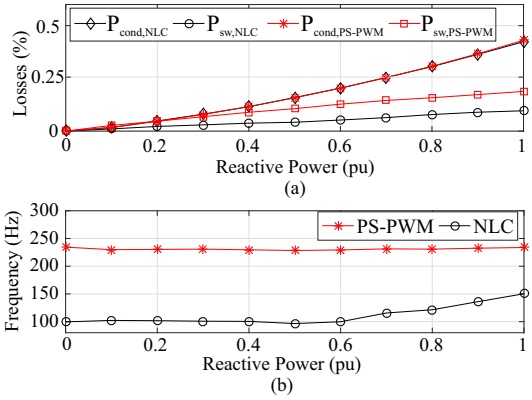

Figure 8: For different operation conditions: (a) Conduction and switching losses; (b) Effective switching frequency.

Fig. 9 shows the mission profiles used for the lifetime analysis. Fig. 9(a) shows the reactive power. This profile is based on measurements in South-eastern Brazil during a week. In the reliability analysis, this profile is replicated over one year. The ambient temperature profile is shown in Fig. 9(b). This profile is also based

on measurements in South-eastern Brazil. However, the measurements were carried out during one year. Also, the data sampling time is 1 second for both profiles.

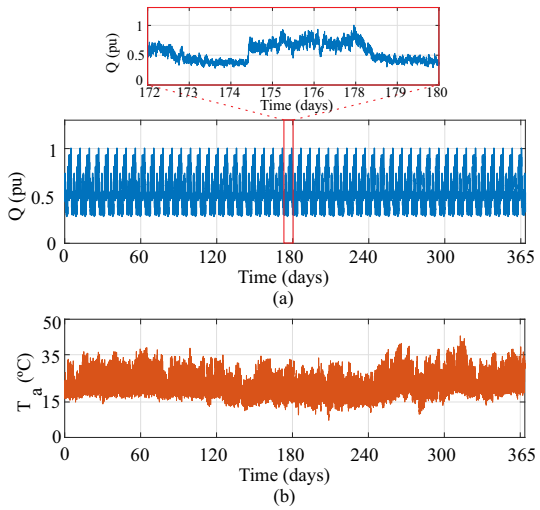

Figure 9: Mission profiles: (a) Reactive Power (S_b = 17 MVar); (b) Ambient Temperature.

Considering the mission profiles, the thermal stresses in each cell power device were obtained. The case temperature of D_2 (most stressed device) for the modulation strategies is shown in Fig 10 for one year and, in detail, for a week. As observed in the zoomed view, the PS-PWM presents the higher case temperature, and also the higher temperature variation in one week.

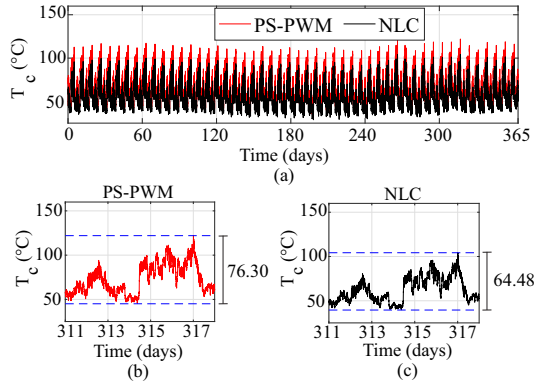

Figure 10: Case Temperature of diode D_2 during: (a) one year for both modulations strategies; (b) one week for PS-PWM; (b) one week for NLC.

The static life consumptions for the bondewire, base plate and chip solder are obtained (Fig. 11) using the lifetime model (see Fig. 7) and Eq. (1). As observed, PS-PWM has higher LC in all devices. In addition, the higher LC is found for the base plate, as illustrated in Fig. 11(b). Therefore, the following evaluations only considered LC in this device part.

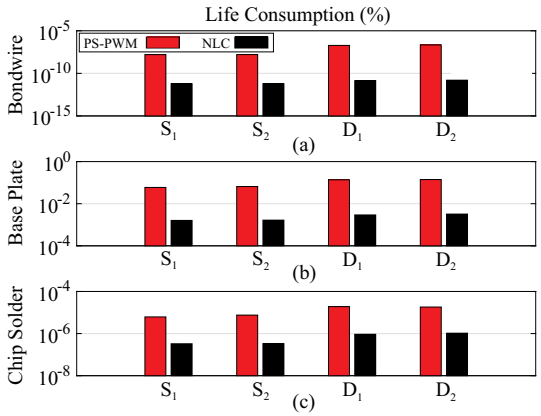

Figure 11: Life Consumption in the cell power devices for both modulation strategies (in semi-logarithmic scale).

Furthermore, considering the static damage in base plate and the methodology employed in [21], the equivalent static values for each semiconductor device and modulation are determined. The Weibull distribution PDF is obtained employing the static values into Monte Carlo simulation with 5% variation.

Due to the fact that D_2 has the highest LC, as shown in Fig. 11, it is presented in Fig. 12 the Weibull distribution PDF only for D_2, since it is the most relevant result. Fig. 12 shows that the modulation strategy may cause a large impact on MMC lifetime distribution, since NLC presents a PDF longer than that of PS-PWM.

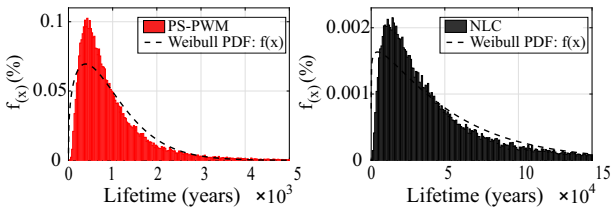

Figure 12: Weibull distribution PDF for D_2

Regarding the lifetime, Fig. 13 shows the results of the unreliability functions. As observed, the diode D_2 has lower lifetime into the component-level for both modulations strategies. This is already expected, since D_2 is the most stressed device in the cell. Concerning the cell-level, considering the 10% failure rate approach, the PS-PWM presents the lifetime of the cell in 99.5 years, while NLC has 2550 years.

Based on cell-level, the system-level reliability assessment is obtained, as illustrated in Fig. 14. Also,

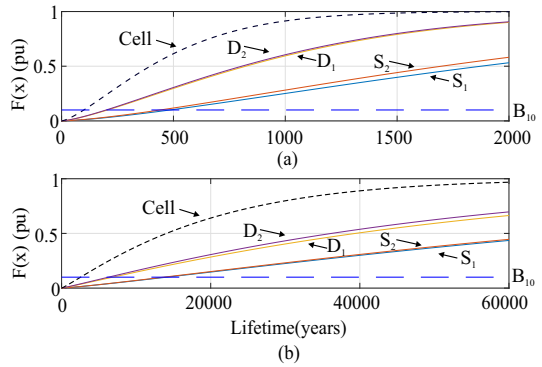

Figure 13: Unreliability function of the cell with the modulation: (a) PS-PWM; (b) NLC.

as observed, for any proportion of failure $F_{MMC}(x)$ the PS-PWM has the lowest lifetime.

Table 1 shows the time with the probability of 1%, 5% and 10% of the population is failed (B_x) for each modulation strategy. As observed, for each percentage of failure, the NLC has higher lifetime. Also, Table 1 presents the lifetime extension related of the NLC. For instance, NLC presents lifetime 10.6 times longer than PS-PWM for B_{10}.

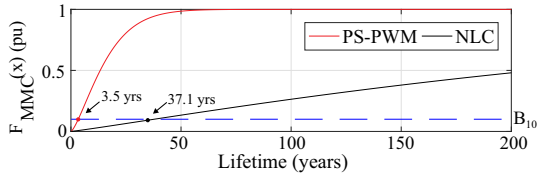

Figure 14: Unreliability function of the MMC.

Table 1: Lifetime Evaluation Results

B_x lifetime	PS-PWM	NLC	Lifetime extension
B_1 (years)	0.6	4.5	7.50
B_5 (years)	1.98	19.5	9.85
B_{10} (years)	3.5	37.1	10.60

Finally, regarding the annual energy consumption, PS-PWM results in 458 MWh of energy losses while NLC results in 348 MWh. Therefore, the use of NLC instead of PS-PWM results in a reduction of 31.4% in energy consumption.

5. Conclusions

This work aimed to compare the modulation strategies PS-PWM and NLC in DSCC-MMC STATCOM application. This comparison was focused on power losses and lifetime evaluation of the power devices.

Regarding power losses, both strategies have similar conduction losses. However, PS-PWM has almost twice more switching losses. As a result, for the mission profiles studied, the PS-PWM has annual energy consumption 31.4% higher than NLC.

Regarding the lifetime evaluation, all results show superior performance for modulation NLC. Indeed, in cell-level and system-level, the NLC has lifetime 25.6 and 10.6 times longer then PS-PWM, respectively.

Therefore, it is possible to infer that the use of NLC modulation strategy is more economically viable. In fact, considering that the costs of implementation of both strategies are similar, the NLC modulation presents clear advantages related with reduced thermal stresses, reduced power losses and extended lifetime of the converters power modules.

6. Acknowledgements

The authors would like to thank to CNPQ, FAPEMIG and CAPES for their assistance and financial support.

References

[1] Q. Wu, J. I. B. Solanas, H. Zhao, . H. Kocewiak, Wind power plant voltage control optimization with embedded application of wind turbines and statcom, in: 2016 Asian Conference on Energy, Power and Transportation Electrification (ACEPT), 2016, pp. 1–5.

[2] Y. Ma, A. Huang, X. Zhou, A review of statcom on the electric power system, in: 2015 IEEE International Conference on Mechatronics and Automation (ICMA), 2015, pp. 162–167.

[3] B. Singh, R. Saha, A. Chandra, K. Al-Haddad, Static synchronous compensators (statcom): a review, IET Power Electronics 2 (4).

[4] E. E. C. Moraes, S. J. de Mesquita, R. P. S. Le£o, M. B. M. Neto, K. Q. da Silva, R. M. C. Correa, H. A. dos Santos, L. Cajuaz, K. P. dos Santos, F. R. Leite, The application of d-statcom in smart distribution grid with wind power plants, in: 2012 10th IEEE/IAS International Conference on Industry Applications, 2012, pp. 1–6.

[5] G. Tsolaridis, H. A. Pereira, A. F. Cupertino, R. Teodorescu, M. Bongiorno, Losses and cost comparison of ds-hb and sd-fb mmc based large utility grade statcom, in: 2016 IEEE 16th International Conference on Environment and Electrical Engineering (EEEIC), 2016, pp. 1–6.

[6] S. Debnath, J. Qin, B. Bahrani, M. Saeedifard, P. Barbosa, Operation, control, and applications of the modular multilevel converter: A review, IEEE Transactions on Power Electronics 30 (1) (2015) 37–53.

[7] M. A. Perez, S. Bernet, J. Rodriguez, S. Kouro, R. Lizana, Circuit topologies, modeling, control schemes, and applications of modular multilevel converters, IEEE Transactions on Power Electronics 30 (1) (2015) 4–17.

[8] K. Sharifabadi, L. Harnefors, H. Nee, S. Norrga, R. Teodorescu, Design, Control, and Application of Modular Multilevel Converters for HVDC Transmission Systems, Wiley - IEEE, Wiley, 2016.

[9] H. A. Pereira, A. F. Cupertino, L. S. Xavier, A. Sangwongwanich, L. Mathe, M. Bongiorno, R. Teodorescu, Capacitor voltage balance performance comparison of mmc-statcom using nlc and ps-pwm strategies during negative sequence current injection, in: 2016 18th European Conference on Power Electronics and Applications (EPE'16 ECCE Europe), 2016, pp. 1–9.

[10] H. Liu, K. Ma, F. Blaabjerg, Device loading and efficiency of modular multilevel converter under various modulation strategies, in: 2016 IEEE 7th International Symposium on Power Electronics for Distributed Generation Systems (PEDG), 2016, pp. 1–7.

[11] A. Marquez, J. I. Leon, S. Vazquez, L. G. Franquelo, M. Perez, A comprehensive comparison of modulation methods for mmc converters, in: IECON 2017 - 43rd Annual Conference of the IEEE Industrial Electronics Society, 2017, pp. 4459–4464.

[12] A. F. Cupertino, J. V. M. Farias, H. A. Pereira, S. I. Seleme, R. Teodorescu, Dscc-mmc statcom main circuit parameters design considering positive and negative sequence compensation, Journal of Control, Automation and Electrical Systems.

[13] K. Ilves, L. Harnefors, S. Norrga, H. P. Nee, Analysis and operation of modular multilevel converters with phase-shifted carrier pwm, IEEE Transactions on Power Electronics 30 (1) (2015) 268–283.

[14] A. Lesnicar, R. Marquardt, An innovative modular multilevel converter topology suitable for a wide power range, in: 2003 IEEE Bologna Power Tech Conference Proceedings,, Vol. 3, 2003, pp. 6 pp. Vol.3–.

[15] F. Sasongko, K. Sekiguchi, K. Oguma, M. Hagiwara, H. Akagi, Theory and experiment on an optimal carrier frequency of a modular multilevel cascade converter with phase-shifted pwm, IEEE Transactions on Power Electronics 31 (5) (2016) 3456–3471.

[16] J. Qin, M. Saeedifard, Reduced switching-frequency voltage-balancing strategies for modular multilevel hvdc converters, IEEE Transactions on Power Delivery 28 (4) (2013) 2403–2410.

[17] S. Kouro, R. Bernal, H. Miranda, C. A. Silva, J. Rodriguez, High-performance torque and flux control for multilevel inverter fed induction motors, IEEE Transactions on Power Electronics 22 (6) (2007) 2116–2123.

[18] Q. Tu, Z. Xu, Power losses evaluation for modular multilevel converter with junction temperature feedback, in: 2011 IEEE Power and Energy Society General Meeting, 2011, pp. 1–7.

[19] K. Ma, N. He, M. Liserre, F. Blaabjerg, Frequency-domain thermal modeling and characterization of power semiconductor devices, IEEE Transactions on Power Electronics 31 (10) (2016) 7183–7193.

[20] H. Huang, P. A. Mawby, A lifetime estimation technique for voltage source inverters, IEEE Transactions on Power Electronics 28 (8) (2013) 4113–4119.

[21] A. Sangwongwanich, Y. Yang, D. Sera, F. Blaabjerg, Lifetime evaluation of grid-connected pv inverters considering panel degradation rates and installation sites, IEEE Transactions on Power Electronics 33 (2) (2018) 1225–1236.

[22] ABB Application note., Load-cycling Capability of Hi-Pak IGBT Modules..

[23] K. E. Hokanson, A. Bar-Cohen, A shear based optimization of adhesive thickness for die bonding, in: Proceedings of 1994 4th Intersociety Conference on Thermal Phenomena in Electronic Systems (I-THERM), 1994, pp. 126–132.

[24] Y. Zhang, H. Wang, Z. Wang, Y. Yang, F. Blaabjerg, The impact of mission profile models on the predicted lifetime of igbt modules in the modular multilevel converter, in: IECON 2017 - 43rd Annual Conference of the IEEE Industrial Electronics Society, 2017, pp. 7980–7985.

[25] P. D. Reigosa, H. Wang, Y. Yang, F. Blaabjerg, Prediction of bond wire fatigue of igbts in a pv inverter under a long-term operation, IEEE Transactions on Power Electronics 31 (10) (2016) 7171–7182.